Influence of Zonal Mean Flow Change on Stationary Wave Fluctuations

IN-SIK KANG

Department of Atmospheric Sciences, College of Natural Sciences, Seoul National University, Seoul, Korea

(Manuscript received 2 March 1989, in final form 17 July 1989)

ABSTRACT

The fluctuation of stationary waves caused by zonal mean flow changes is investigated using a barotropic model and GCM simulated upper-level data. The EOF analysis of monthly mean $\bar{u}$ fluctuations during winter shows that a positive anomaly at the jet stream accompanies a negative anomaly of zonal mean flow in the high latitudes. The typical magnitudes of the anomalous zonal mean flow are 5 and 8 m s^{-1} in the jet stream latitudes and in the high latitudes, respectively.

With these fluctuations of the basic state, the wave propagation characteristics are significantly modified from month to month. The zonal mean flow changes subject to fixed large-scale mountains result in a large part of the stationary wave fluctuations. It is also demonstrated that the precise location of the turning latitude plays an important role in the pattern of stationary wave responses to a fixed forcing.

1. Introduction

The nature and causes of stationary wave fluctuations have been important subjects in climate research, because of their profound impact on regional climate. Although a number of dynamical mechanisms, for example, those reviewed by Wallace and Blackmon (1983), can cause the fluctuations, fluctuations of sea surface temperature and zonal mean flow have been suggested to be primary factors (Kang and Lau 1986). In the present study we investigate the influence of zonal mean flow on the stationary wave fluctuations by the use of a linear barotropic model and two-dimensional Rossby wave dynamics.

The relationship between the zonal mean flow and the stationary waves was first discussed by Rossby (1939). Using his well-known dispersion relationship for one-dimensional waves in a barotropic atmosphere, he postulated that the semi-permanent Aleutian low should tend to drift westward during periods of weak zonal mean flow and vice versa. Namias (1950) also showed a qualitative relationship between the zonal index, defined by the difference between zonal mean sea-level pressure at 35°N and that at 55°N, and many features of the global circulation. The alternating appearance of high and low zonal mean flow in the mid-latitudes, the so-called "index cycle," was viewed in early studies by Rossby and Willett (1950) as resulting from the combined action of cyclone activity and north–south diabatic heating gradient.

Several recent studies (e.g., Branstator 1984; Kang and Lau 1986; Tung and Rosenthal 1987; Nigam and Lindzen 1989) also have demonstrated the importance of zonal mean flow on the stationary wave fluctuations. In particular, by analyzing a 15-year GCM data, Kang and Lau showed that one of the predominant modes of stationary wave fluctuations during northern winter is associated with fluctuations of zonal mean flow. They further demonstrate that the principal mode of circulation anomaly appearing in the experiment by Lau (1981) is actually associated with the principal mode of zonal mean flow fluctuations. Branstator (1984) has tested the relationship between fluctuations of zonal mean flow and the corresponding fluctuations of stationary wave using observed climatological data which covers the area north of 20°N. He simulated reasonably well the anomalous stationary waves associated with the change of zonal mean flow by the use of a linear barotropic model.

The present study investigates the zonal-eddy relationship appearing in a 15-year GCM experiment with a similar approach to that used by Branstator. But this study further tests the influence of the meridional structure of the zonal mean flow on the propagation characteristics and thus the horizontal structure of planetary-scale waves. In particular, it is demonstrated that the fluctuation of the turning latitude of the wave has a large effect on the amplitude and pattern of anomalous stationary waves in the middle and high latitudes.

2. Data

The data used in the present study is obtained from a 15-year GCM experiment conducted at Geophysical

Corresponding author address: Prof. In-Sik Kang, Dept. of Atmospheric Sciences, College of Natural Sciences, Seoul National University, Seoul 151, Korea.

Fluid Dynamics Laboratory (GFDL). In the GCM the model variables are represented in terms of spherical harmonics with rhomboidal truncation at wavenumber 15 in the horizontal and 9 sigma levels in the vertical. In the GCM experiment, no interannual variability of external forcing (e.g., insolation and sea surface temperature) has been introduced. The detailed description of the experiment, the so-called "control run," can be found in Lau (1981) and Kang and Lau (1986). From the historical tapes produced by the experiment, the monthly mean wind field at 300 mb level during northern winter is extracted. From the wind field, 45 monthly means of zonal mean zonal wind ($\bar{u}$), eddy streamfunction (Ψ^*), and divergence (D) are calculated and utilized in the present study.

3. Principal mode of zonal mean flow fluctuations

Using empirical orthogonal function (EOF) analysis, Kang and Lau (1986) obtained the principal mode of zonal mean flow fluctuations. Their principal eigenvector $e_1(\bar{u})$ and the associated time series $c_1(\bar{u})$ are reconstructed and shown in Figs. 1 and 2, respectively. The first eigenvector explains 39.2% of the total variance of zonal mean flow in the Northern Hemisphere. Figure 1 shows that the fluctuation of zonal mean flow near 30°N is negatively correlated with the corresponding fluctuations at high latitudes and tropics. This eigenvector is similar to the observed counterpart obtained by Branstator (1984).

The typical amplitude of zonal mean flow change associated with $e_1(\bar{u})$ is illustrated in the composite map shown in Fig. 3. In the figure, the composite $\bar{u}_1$ is constructed by averaging the zonal mean flow for the 7 winter months with most positive value of $c_1(\bar{u})$, indicated in Fig. 2 by stippled columns, and $\bar{u}_2$ is the average for the 7 months with most negative value of $c_1(\bar{u})$, indicated by stripped columns. Composite $\bar{u}_1$ shows a strong jet stream in the subtropics and a sharp meridional gradient in the extratropics. On the other hand, $\bar{u}_2$ is characterized by a smoother meridional structure. The difference between $\bar{u}_1$ and $\bar{u}_2$ has the same meridional structure as that of $e_1(\bar{u})$, and the amplitude of the difference is about 5 m s^{-1} near the jet stream latitude and about 8 m s^{-1} near 55°N.

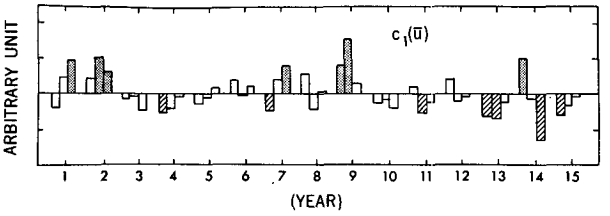

FIG. 2. Time series associated with the first eigenvector shown in Fig. 1. Those 7 months with the most positive (negative) values are indicated by stippled (stripped) columns. Tick marks along the x-axis indicate the January of each year.

The anomalous eddy streamfunction associated with the change of zonal mean flow is shown in Fig. 4. This map has been obtained by subtracting the composite eddy streamfunction associated with $\bar{u}_2$ from the composite associated with $\bar{u}_1$. The composite procedure is the same as that for $\bar{u}$. In the figure, large wave trains are evident in the Pacific and Atlantic. The amplitude of the anomalous streamfunction is comparable to that of the anomaly during an El Niño event. In section 4, we examine the extent to which the anomalous eddy streamfunction is associated with the zonal mean flow change shown in Fig. 3.

4. Barotropic model results

Though the anomalous eddy streamfunction shown in Fig. 4 is likely associated with the change of zonal mean flow, it is also possible that the association may not be a result of mutual adjustment of Ψ^* and $\bar{u}$. One of the other possibilities is that changes of the stationary waves and zonal mean flow are both caused by different states of transient activity. The present study, however, tests the simple linear adjustment hypothesis; that is, we examine the extent to which the anomalous streamfunction is simulated by simple linear models with different basic states.

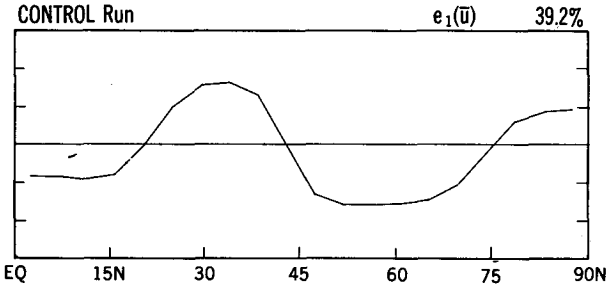

FIG. 1. First eigenvector of the zonally averaged zonal wind at 300 mb, $e_1(\bar{u})$, as computed using the 45 winter monthly means of the 15-year GCM experiment.

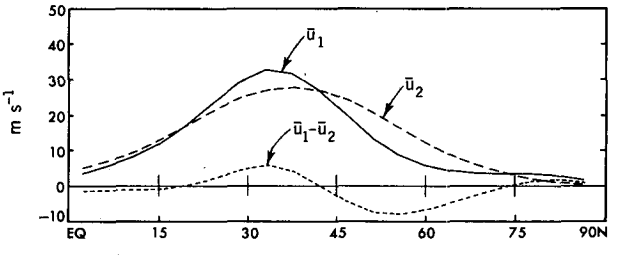

FIG. 3. Composites of zonal mean flow: $\bar{u}_1$ is constructed by averaging the zonal mean flow for the 7 months with most positive value of $c_1(\bar{u})$, indicated in Fig. 2 by stippled columns, and $\bar{u}_2$ is the average for the 7 months with most negative value of $c_1(\bar{u})$, indicated by stripped columns.

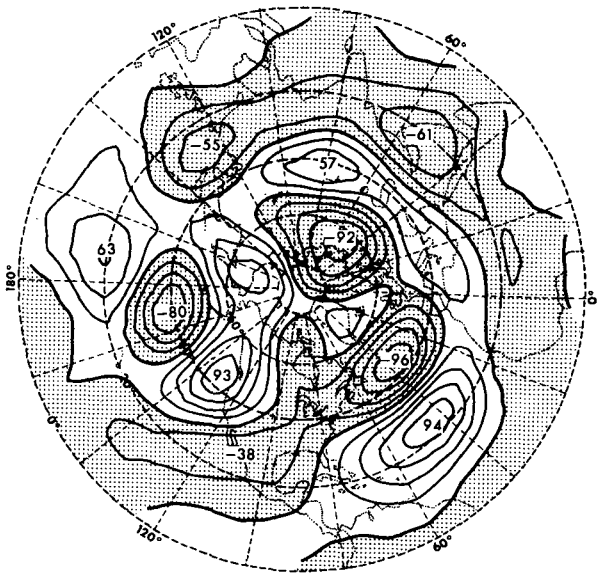

FIG. 4. Anomalous eddy streamfunction obtained by subtracting the composite eddy streamfunction associated with $\bar{u}_2$ from the composite associated with $\bar{u}_1$. The composite procedure is the same as that used in Fig. 3. Contour interval is 2×10^6 m^2 s^{-1}.

The model used in this study is constructed with the nondivergent barotropic vorticity equation linearized about a zonal mean flow, which can be written as

$$\frac{\partial \zeta^*}{\partial t} + \frac{\bar{u}}{a\cos\phi}\frac{\partial \zeta^*}{\partial \lambda} + \frac{1}{a\cos\phi}\frac{\partial \Psi^*}{\partial \lambda}\frac{\partial \bar{\eta}}{a\partial\phi} = F + D \quad (1)$$

where $\zeta = \nabla^2\Psi$ is the relative vorticity, η the absolute vorticity, u the zonal velocity, λ the longitude, ϕ the latitude, and a the earth's radius. The overbar denotes the zonal mean and the superscript star the deviation from the mean; F represents the vorticity forcing which can be induced by divergence or by orography. The dissipation term D includes the following two processes.

$$D = -\kappa\zeta^* - \alpha\nabla^4\zeta^*$$

where κ is the linear drag coefficient, the value of $(10\ \text{d})^{-1}$ is used in the present model. The biharmonic horizontal diffusion is included with the same form as used in the GCM. The coefficient $\alpha = 1 \times 10^{16}$ m^4 s^{-1}. The diffusion process is very scale dependent and thus negligibly affects the large-scale solutions of the present model. The variable ζ^* is represented in terms of orthogonal spherical harmonics. As in the GCM, the sum of spherical harmonics is truncated at rhomboidal wavenumber 15.

For a fixed forcing, two barotropic models with prescribed zonal mean flows $\bar{u}_1$ and $\bar{u}_2$, respectively, are separately integrated from zero initial state up to day 40. After 20 days of integration the pattern of the response does not change significantly, indicating that a quasi-steady state has been reached. For the purpose of presentation, the time mean fields of the last 20 days of integration are computed and displayed in this paper.

The first experiment is performed with the following climatological vorticity forcing,

$$F = -[(\zeta_c + f)D_c]^*$$

where ζ_c and D_c are, respectively, the 15-year winter mean vorticity and divergence obtained from the GCM, and f denotes the Coriolis parameter.

Barotropic models with the basic states $\bar{u}_1$ and $\bar{u}_2$ produce eddy streamfunctions, $\Psi^*(\bar{u}_1)$ and $\Psi^*(\bar{u}_2)$, respectively. The difference between the two model results is shown in Fig. 5. This figure may be compared with the GCM counterpart shown in Fig. 4. There are some discrepancies between the two maps; in particular, the low located in the mid-Pacific shown in Fig. 4 is shifted to the northwest in the simulation. In general, however, the linear model reasonably well reproduces the GCM anomalous streamfunction. Taking into account the simplicity of the present model, this result suggests that a large fraction of the anomalous eddy streamfunction can be explained in this linear framework as the adjustment of Ψ^* to $\bar{u}$.

In the second experiment, the forcing term of the model is replaced by the following topographic forcing.

$$F = -\frac{f}{h_0}\frac{\bar{u}}{a\cos\phi}\frac{\partial h_T}{\partial \lambda}$$

where $h_0 = 8$ km is the scale height of the atmosphere, and h_T the height of topography over the globe.

The difference map of streamfunction obtained from the two linear model runs with the basic states $\bar{u}_1$ and

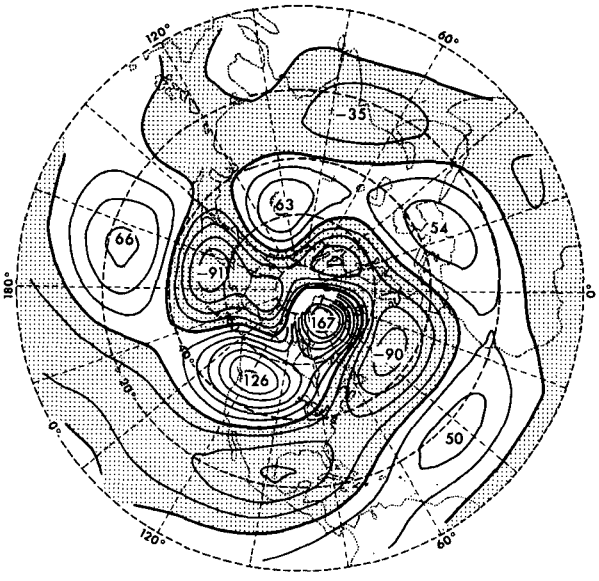

FIG. 5. Anomalous eddy streamfunction produced by the difference of two linear barotropic model results. The barotropic models with two basic states $\bar{u}_1$ and $\bar{u}_2$ are both forced by the same climatological vorticity forcing. Contour interval is 2×10^6 m^2 s^{-1}.

$\bar{u}_2$ but with the same topography is shown in Fig. 6. In this figure, the downstream anomaly forced by the Himalaya mountains is particularly pronounced in the Pacific sector, but in the western hemisphere the mountain induced anomaly is fairly weak compared with the GCM counterpart. Although the low in the mid-Pacific shown in Fig. 4 is still shifted northwestward, the general pattern of the wave train in the Pacific and North American sector is similar to the GCM counterpart and that shown in Fig. 5. This result suggests that a large fraction of the anomalous eddy streamfunction in the Pacific and North American region is a result of differences in the wave trains induced by the same mountain but propagated through different zonal mean flows.

5. Idealized case

In section 4, it is shown that two different basic states produce different wave trains for the same atmospheric forcing, and consequently that the change of the zonal mean flow itself can cause significant anomalous circulation in the atmosphere. We now investigate how the horizontal structure of the wave train is determined by the basic states, $\bar{u}_1$ and $\bar{u}_2$, by examining the Rossby wave ray theory (e.g., Hoskins and Karoly 1981; Held 1983) and the responses of the linear barotropic model to idealized vorticity sources.

a. Theoretical preliminary

In the Mercator projection of the sphere, the linearized vorticity equation (1) for a steady state can be written as

$$\bar{u}_M \frac{\partial}{\partial x} \nabla^2 \Psi^* + \beta_M \frac{\partial \Psi^*}{\partial x} = 0 \qquad (2)$$

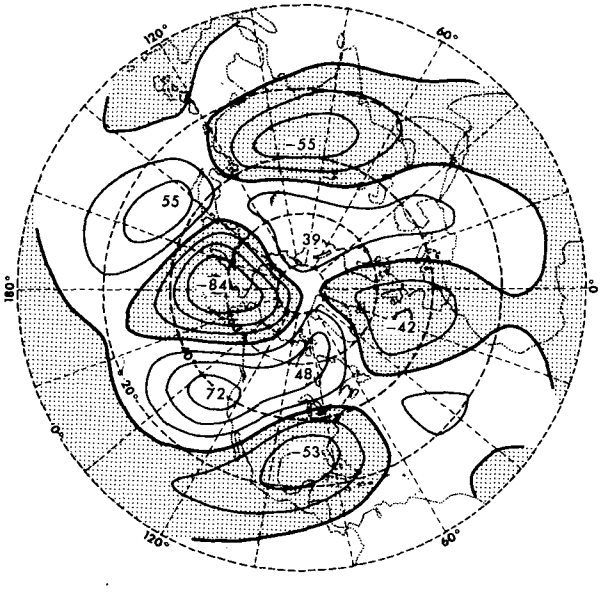

FIG. 6. As in Fig. 5, except the topographic forcing.

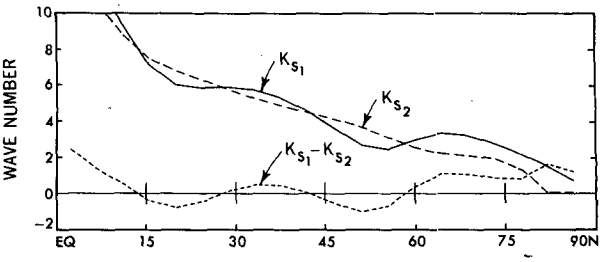

FIG. 7. Meridional structures of the stationary wavenumber K_S multiplied by the earth's radius for the zonal mean flows $\bar{u}_1$ and $\bar{u}_2$.

where $x = a\lambda$, $y = a \ln[(1 + \sin\phi)/\cos\phi]$, and $\bar{u}_M = \bar{u}/\cos\phi$, $\beta_M = \frac{d}{dy}(f - d\bar{u}/dy)$. Introducing a wave solution $\Psi = \tilde{\Psi}(y)e^{ikx}$ into Eq. (2), we obtain the following equation.

$$\frac{d^2\tilde{\Psi}}{dy^2} + (K_S^2 - k^2)\tilde{\Psi} = 0 \qquad (3)$$

where $K_S = (\beta_M/\bar{u}_M)^{1/2}$ is the stationary wavenumber. Equation (3) gives a criterion for meridional propagation of the wave. If $K_S > k$ the wave can propagate meridionally, but at latitudes where $K_S < k$ it is exponentially damped. In the above the stationary wavenumber is solely determined by the meridional structure of the zonal mean flow, and the ray amplitude of wavenumber k depends on the magnitude of forcing projected onto the wavenumber space k and the medium through which the wave propagates. The WKB theory tells that

$$\Psi \approx \frac{1}{\sqrt{l}} \exp[i(kx + \int^y l\,dy)] \qquad (4)$$

where $l^2 = K_S^2 - k^2$. Thus the wave amplitude is proportional to $l^{-1/2}$, and at the turning latitude where $K_S = k$, the amplitude becomes infinity. However, this formula breaks down near the turning point, where the WKB solution must be matched to the decaying solution on the other side and the solution is expressed in terms of Airy functions. But the amplitude still reaches its maximum near the turning point. Overall, the meridional structure of K_S is the *only* factor that determines the propagation characteristics and amplitude of the wave forced by a given forcing.

The meridional structures of K_S multiplying by the earth's radius for the zonal mean flows $\bar{u}_1$ and $\bar{u}_2$ denoted by K_{S_1} and K_{S_2}, respectively, are shown in Fig. 7. The major differences between the two K_S curves are in middle and high latitudes; K_{S_2} is bigger than K_{S_1} in midlatitudes while the reverse is true in high latitudes. For instance, when a planetary-scale wave (e.g., of wavenumber 3) is incident from the subtropics, the wave can propagate to midlatitudes in both basic states, but the basic state $\bar{u}_2$ allows the wave to propagate farther to the north than $\bar{u}_1$ does.

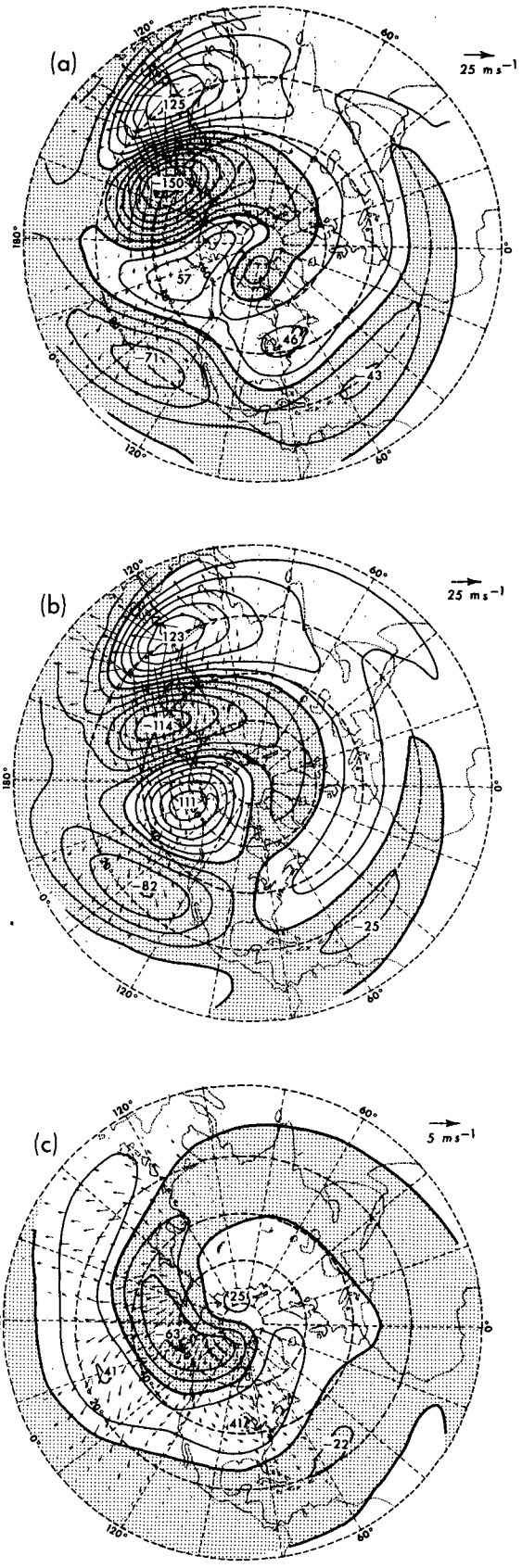

b. The model responses to idealized vorticity sources

We now examine the linear barotropic model responses to idealized vorticity sources located at various latitudes. The following elliptical formula is used for the forcing function.

$$F(\lambda, \phi) = \begin{cases} A\left[\sin\dfrac{\pi(\phi-\phi_1)}{(\phi_2-\phi_1)}\sin\dfrac{\pi(\lambda-\lambda_1)}{(\lambda_2-\lambda_1)}\right], \\ \quad \text{for } \lambda_1 < \lambda < \lambda_2 \text{ and } \phi_1 < \phi < \phi_2 \\ 0, \quad \text{otherwise,} \end{cases}$$

where $A = -1 \times 10^{-10}\ \mathrm{s}^{-1}$, $\lambda_1 = 160°\mathrm{E}$, $\lambda_2 = 100°\mathrm{E}$, and $\phi_1 = \phi_0 - 10°$, $\phi_2 = \phi_0 + 10°$, where ϕ_0 is the latitude of the maximum forcing.

For the idealized vorticity source centered at 20°N, the streamfunction responses of the model with basic states $\bar{u}_1$ and $\bar{u}_2$, respectively, are shown in Figs. 8a and 8b. Both figures are characterized by a wave train with a great circle path emanating from the source region. The wave trains are more clearly represented by the two-dimensional wave flux vector $\mathbf{F}_S$ (arrows in the figures) formulated by Plumb (1985). This wave flux vector is defined as

$$\mathbf{F}_S \approx \begin{pmatrix} \dfrac{1}{2a^2\cos^2\phi}\left[\left(\dfrac{\partial\Psi^*}{\partial\lambda}\right)^2 - \Psi^*\dfrac{\partial^2\Psi^*}{\partial\lambda^2}\right] \\ \dfrac{1}{2a^2\cos\phi}\left[\dfrac{\partial\Psi^*}{\partial\lambda}\dfrac{\partial\Psi^*}{\partial\phi} - \Psi^*\dfrac{\partial^2\Psi^*}{\partial\lambda\partial\phi}\right] \end{pmatrix}$$

The vector $\mathbf{F}_S$ is parallel to the group velocity of stationary waves. The divergence and convergence of the flux vector are, respectively, related to the generation and dissipation of wave activity.

In the figures the forced responses near the source are similar to each other, because of negligible difference between $\bar{u}_1$ and $\bar{u}_2$ at 20°N. The local responses can be explained in terms of steady-state vorticity balance. In the subtropics near 20°N, where the zonal mean flow is relatively large, both advection terms, the second and third terms in Eq. (1), are important but have opposite signs. Thus west of the source the zonal advection balances the sum of the negative vorticity forcing and planetary vorticity advection, while east of the source the planetary vorticity advection balances the other two terms. Stronger meridional motion is accordingly maintained to the east of the source rather than to the west.

The downstream responses in the two figures, on the other hand, exhibit certain differences. As indicated earlier in this section, the planetary-scale waves prop-

FIG. 8. Streamfunction responses to the idealized vorticity forcing centered at 20°N. (a) is the response of the model with the basic state $\bar{u}_1$, and (b) for the model with the basic state $\bar{u}_2$; (c) shows the anomalous streamfunction, (a) minus (b). Contour interval is 2×10^6 $\mathrm{m}^2\ \mathrm{s}^{-1}$. Arrows indicate the wave flux vector as obtained using Eq. (5).

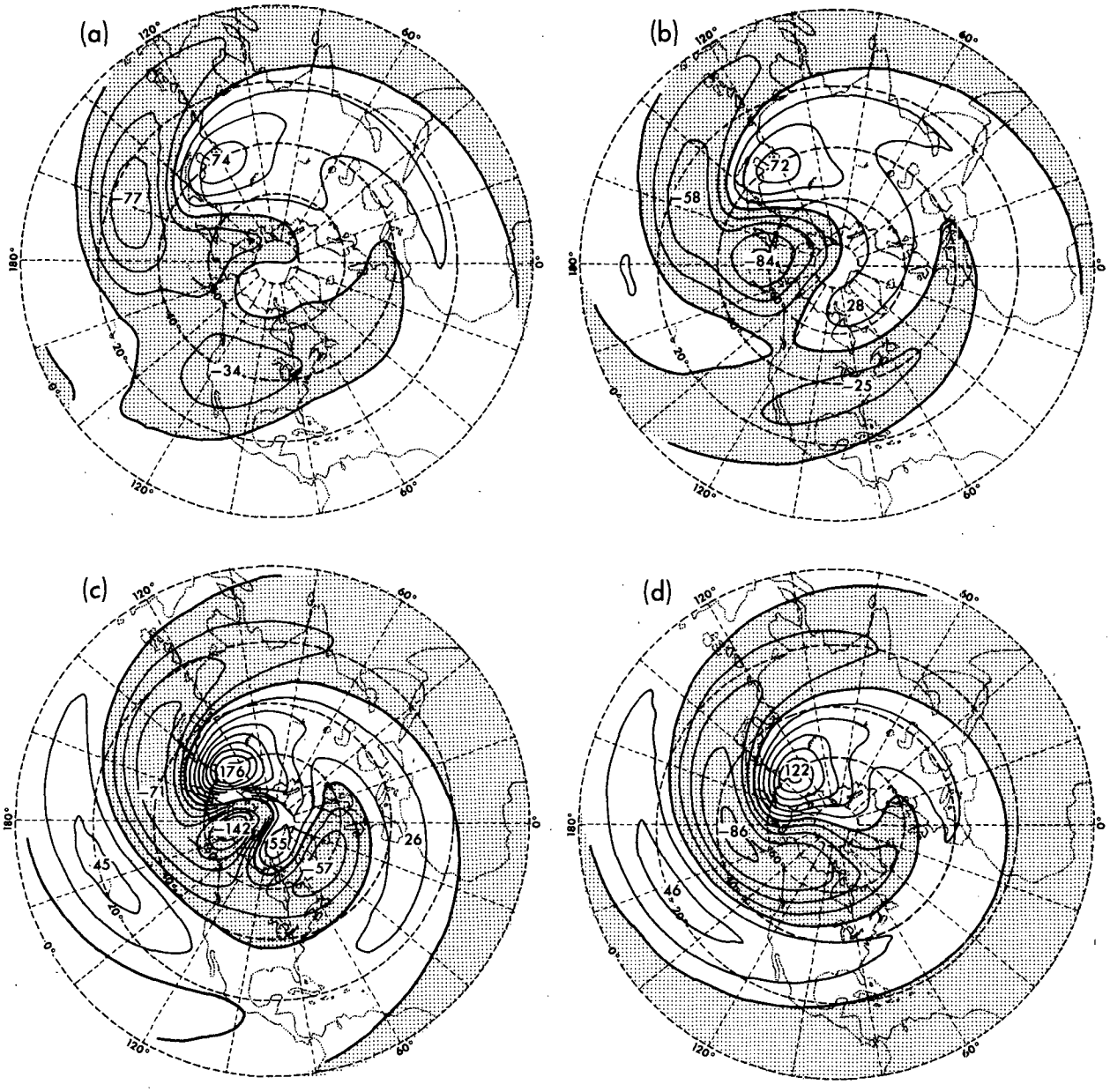

FIG. 9. As in Fig. 8, but (a) for the basic state $\bar{u}_1$ and the forcing at 40°N; (b) for $\bar{u}_2$ and the forcing at 40°N; (c) for $\bar{u}_1$ and the forcing at 60°N; (d) for $\bar{u}_2$ and the forcing at 60°N.

agating through the basic state $\bar{u}_1$ hit a turning latitude in midlatitudes, resulting in the maximum response near 40°N. But the $\bar{u}_2$ basic state allows wave propagation farther to the north. The different characteristics of wave propagation are well represented by the wave flux vectors in the figures. In particular, noted differences can be found in the Pacific region between 40° and 60°N where the turning point exists.

Figure 8c clearly shows that the anomalous streamfunction, Fig. 8a minus Fig. 8b, is pronounced in the Pacific region remote from the source. Although the anomalous wave train seems to originate at high latitudes and the group velocity is directed to the south, the anomalous wave is a result of the difference in propagation of the waves incident from the subtropics. It may be important to note that the anomaly is strongly determined by the different locations of the turning latitude.

The model responses to the forcing centered at 40°N are shown in Figs. 9a and 9b, respectively, for the basic states $\bar{u}_1$ and $\bar{u}_2$. As indicated in Fig. 7, the waves superimposed on the $\bar{u}_1$ basic state can hardly propagate to the north, but they propagate to the south. On the other hand, the $\bar{u}_2$ basic state allows the waves to propagate to the high latitudes as well as to the south. In Fig. 9b, the northward propagating wave hits the turn-

ing latitude near 60°N, resulting in a large response there.

The waves forced by the vorticity source centered at 60°N, shown in Figs. 9c and 9d, have different propagating characteristics compared with those forced by the 40°N forcing. For the basic state $\bar{u}_1$, waves favorably propagate northward (Fig. 9c), but the basic state $\bar{u}_2$ only allows wave propagation to the south (Fig. 9d). The propagation characteristics can be inferred from the latitudinal distributions of stationary wavenumber K_S shown in Fig. 7. Overall, the above idealized experiments show that the different states of zonal mean flow in the high latitudes strongly influence the stationary wave train and thus produce large anomalous circulations.

6. Conclusion

In a long-term GCM integration, the zonal mean flow during northern winter is found to fluctuate significantly. The EOF analysis of monthly mean $\bar{u}$ fluctuations shows that the anomaly near 30°N is negatively correlated with the anomaly in high latitudes and in the tropics. Associated with the zonal mean flow change, the stationary wave component varies from month to month.

In the present study, the linear adjustment process between the changes of $\bar{u}$ and the stationary waves is studied by examining the extent to which the change of stationary waves is simulated by a simple linear model with different states of zonal mean flow. It is shown that the responses of forced Rossby waves depend strongly on the structure of zonal mean flow. In particular, the precise location of the turning latitude plays an important role in determining the pattern and amplitude of remote responses to a fixed forcing in a barotropic model.

The present study may indicate that the correct prediction and simulation of stationary waves require precise information on the zonal mean state. At present, the causes of zonal mean flow fluctuations are not fully understood. Therefore, further research related to this topic should be pursued to improve the long-range prediction of regional atmospheric circulation.

Acknowledgment. The author would like to thank Dr. Isaac M. Held for his careful review of an earlier manuscript which helped much to improve this paper. This work was presented at the Sixth Conference on Atmospheric and Oceanic Waves and Stability held at Seattle, Washington, 25–28 August 1987.

REFERENCES

Branstator, G. W., 1984: The relationship between zonal mean flow and quasi-stationary waves in the midtroposphere. *J. Atmos. Sci.*, **41,** 2163–2178.

Held, I. M., 1983: Stationary and quasi-stationary eddies in the extratropical troposphere: Theory. *Large-Scale Dynamical Processes in the Atmosphere,* Hoskins and Pearce, Eds., Academic Press, 127–168.

Hoskins, B. J., and D. J. Karoly, 1981: The steady linear response on a spherical atmosphere to thermal and orographic forcing. *J. Atmos. Sci.*, **38,** 1179–1196.

Kang, I.-S., and N.-C. Lau, 1986: Principal modes of atmospheric variability in model atmospheres with and without anomalous sea surface temperature forcing in the tropical Pacific. *J. Atmos. Sci.*, **43,** 2719–2735.

Lau, N.-C., 1981: A diagnostic study of recurrent meteorological anomalies appearing in a 15-year simulation with a GFDL general circulation model. *Mon. Wea. Rev.*, **109,** 2287–2311.

Nigam, S., and R. S. Lindzen, 1989: The sensitivity of stationary waves to variations in the basic state zonal flow. *J. Atmos. Sci.*, **46,** 1746–1768.

Namias, J., 1950: The index cycle and its role in the general circulation. *J. Meteor.*, **7,** 130–139.

Plumb, R. A., 1985: On the three-dimensional propagation of stationary waves. *J. Atmos. Sci.*, **42,** 217–229.

Rossby, C. G., 1939: Relations between variations in the intensity of the zonal circulation of the atmosphere and the displacements of the semipermanent centers of action. *J. Mar. Res.*, **2,** 38–55.

——, and H. C. Willett, 1948: The circulation of the upper troposphere and lower stratosphere. *Science,* **108,** 643–652.

Tung, K. K., and A. J. Rosenthal, 1986: On the extended-range predictability of large-scale quasi-stationary patterns in the atmosphere. *Tellus,* **38A,** 333–365.

Wallace, J. M., and M. L. Blackmon, 1983: Observations of low-frequency atmospheric variability. *Large-Scale Dynamical Processes in the Atmosphere,* Hoskins and Pearce, Eds., Academic Press, 55–94.